

Adjustable polarization-independent wide-incident-angle broadband far-infrared absorber

Jiu-Sheng Li(李九生), Xu-Sheng Chen(陈旭生)

Citation: Chin. Phys. B . 2020, 29(7): 078703 . **doi:** 10.1088/1674-1056/ab8892
Journal homepage: http://cpb.iphy.ac.cn; http://iopscience.iop.org/cpb

What follows is a list of articles you may be interested in

Polarization conversion metasurface in terahertz region

Chen Zhou(周晨), Jiu-Sheng Li(李九生)

Chin. Phys. B . 2020, 29(7): 078706 . **doi:** 10.1088/1674-1056/ab9295

Effect of terahertz pulse on gene expression in human eye cells

Jin-Wu Zhao(赵晋武), Ming-Xia He(何明霞), Li-Jie Dong(东莉洁), Shao-Xian Li(李绍限), Li-Yuan Liu(刘立媛), Shao-Chong Bu(步绍翀), Chun-Mei Ouyang(欧阳春梅), Peng-Fei Wang(王鹏驰), Long-Ling Sun(孙珑玲)

Chin. Phys. B . 2019, 28(4): 048703 . **doi:** 10.1088/1674-1056/28/4/048703

Avian magnetoreception model realized by coupling a magnetite-based mechanism with a radical-pair-based mechanism

Lü Yan, Song Tao

Chin. Phys. B . 2013, 22(4): 048701 . **doi:** 10.1088/1674-1056/22/4/048701

SPECIAL TOPIC — Terahertz physics

Adjustable polarization-independent wide-incident-angle broadband far-infrared absorber*

Jiu-Sheng Li(李九生)† and Xu-Sheng Chen(陈旭生)

Centre for THz Research, China Jiliang University, Hangzhou 310018, *China*

(Received 20 February 2020; revised manuscript received 13 March 2020; accepted manuscript online 12 April 2020)

To promote the application of far-infrared technology, functional far-infrared devices with high performance are needed. Here, we propose a design scheme to develop a wide-incident-angle far-infrared absorber, which consists of a periodically semicircle-patterned graphene sheet, a lossless inter-dielectric spacer and a gold reflecting film. Under normal incidence for both TE- and TM-polarization modes, the bandwidth of 90% absorption of the proposed far-infrared absorber is ranging from 6.76 THz to 11.05 THz. The absorption remains more than 90% over a 4.29-THz broadband range when the incident angle is up to 50° for both TE- and TM-polarization modes. The peak absorbance of the absorber can be flexibly tuned from 10% to 100% by changing the chemical potential from 0 eV to 0.6 eV. The tunable broadband far-infrared absorber has promising applications in sensing, detection, and stealth objects.

Keywords: far-infrared absorber, semicircle-patterned graphene, wide incident angle

PACS: 87.50.–a, 87.50.up, 87.10.Vg **DOI:** 10.1088/1674-1056/ab8892

1. Introduction

Due to having the ability to support surface plasmons from terahertz to optical regime, graphene has attracted increasing interests for the application of terahertz and optical devices, such as polarizers,[1] photodetectors,[2] modulators,[3–6] and absorbers.[7–10] Especially, the tunability of its carrier mobility and conductivity, the performance of graphene-based devices can be controlled by chemical doping or electrostatic doping to change the Fermi level without changing the structure of the device. As one of the most important devices, absorbers with different geometries of graphene have been designed including disks and independent ribbon,[11–14] square patch,[15] stack,[16] multi-layered structure,[17,18] and cross-shaped structure.[19,20] In order to increase the absorbance bandwidth, the graphene patterns-based absorbers have been proposed.[21–23] Although the fractional bandwidth of these absorbers based on multi-layered structure can be enhanced, most of the mentioned graphene-based absorbers suffer from some drawbacks, such as the difficulty in fabrication technique, angle dependence, and polarization sensitivity of the incident electromagnetic waves. However, despite recent making some progress in absorbers, these absorbers are designed in the terahertz and optical regions. Furthermore, far-infrared absorbers are rarely reported. As an indispensable frequency band of far-infrared electromagnetic wave, a wide-angle and polarization insensitive broadband far-infrared absorber with single-layer simple patterned graphene still remains worth to be further investigated.

In this study, a periodically semicircle-patterned graphene sheet absorber is proposed to achieve over 90% broadband far-infrared absorption a wide-incident-angle. By introducing gradient width of the semicircle-patterned graphene unit, the continuous plasmon resonances of the far-infrared absorber are directly excited. The bandwidth of 90% absorbance is 4.29 THz from 6.76 THz to 11.05 THz. The absorbance is more than 90% even the incident angles reach 50° for both TE- and TM-polarization modes. The broadband absorption spectra of the far-infrared absorber are insensitive to the polarizations and the incident angles. By tuning the chemical potential via electrostatic doping of the semicircle-patterned graphene sheet, the peak absorption can be continuously controlled from 10% to 100%. This design scheme offers a new perspective on the design of graphene-based tunable far-infrared devices. The proposed absorber has promising applications in far-infrared detecting, sensing, imaging and stealth.

2. Structure design

Figure 1 shows the geometry and unit cell of the proposed far-infrared absorber by depositing the periodically planar arrays of semicircle disk-patterned graphene on polymide substrate. A thin ion gel layer is coated on the top of the semicircle disk-patterned graphene sheet and contacted to the top electrode to control the graphene conductivity via DC voltage. The Au ground plane can be used as another electrode. Figure 1(b) shows the unit cell of the far-infrared absorber, which is composed of four semicircle disks patterned graphene with the same radius and a gold ground plate, separated by a lossless polymide layer. p is the periods in x and y directions, h is the thickness of the dielectric spacer, r is the radius of semicir-

*Project supported by the National Key Research and Development Program of China (Grant No. 2016YFF0200306) and the National Natural Science Foundation of China (Grant Nos. 61871355 and 61831012).

†Corresponding author. E-mail: jshli@126.com

© 2020 Chinese Physical Society and IOP Publishing Ltd

cle disk patterned graphene. We assume the lossless dielectric spacer is polyimide with the permittivity of $\varepsilon = 3.5$. The conductivity of the gold ground plate is $\sigma_{\text{gold}} = 4.56 \times 10^7$ S/m with the thickness of 0.2 μm. The initial values of the structure parameters are set to be $p = 4$ μm, $h = 4.6$ μm, $t = 10$ nm, and $r = 1.2$ μm. The thickness of the graphene sheet is set to 1 nm for easy simulation.[24] The semi-circle graphene patterns can be fabricated by large-scale synthesis, transfer and etching techniques, and the electron beam lithography can be employed to produce semi-circle patterns on graphene layer. The chemical vapor deposition method is one of the beneficial methods for fabricating this multilayer structure.

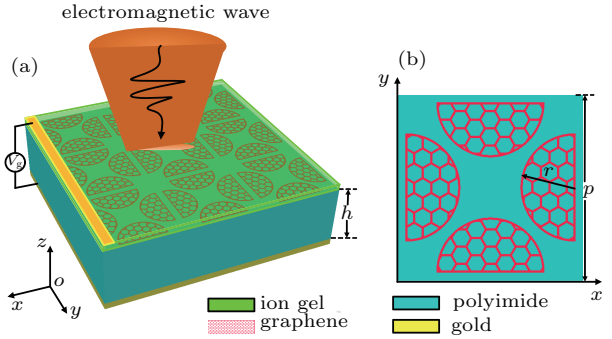


Fig. 1. (a) Schematic diagram of the proposed far-infrared absorber and (b) top-view of the semicircle disk-patterned graphene unit cell.

In our proposed structure, the lateral-view of the semicircle disk-patterned graphene likes a graphene ribbon with a gradient along width direction. When the graphene ribbon has a width (W) and is excited by a normal incident electrical vector, it will produce significant plasmon resonance, which appears in Ref. [21]

$$W = (1 - \phi/\pi)\,\lambda_{\text{eff}}/2, \tag{1}$$

where ϕ is the phase of the plasmon resonance reflection coefficient, λ_{eff} is the effective resonant wavelength determined by $\lambda_{\text{eff}} = \lambda_0/\text{Re}(n_{\text{eff}})$, and λ_0 is the vacuum wavelength. According to the principle of bubble incompatibility, when the photon energy is $\hbar\omega \ll E_{\text{f}}$, the influence of the conductivity between bands is negligible, $\text{Re}(n_{\text{eff}}) \approx \hbar\omega/(2\alpha E_{\text{f}})$,[25] where α is a fine structural constant. The resonant frequency can be obtained by

$$f = \sqrt{c\alpha E_{\text{f}}(1 - \phi/\pi)/(2\pi\hbar W)} \propto \sqrt{E_{\text{f}}/W}, \tag{2}$$

where c is the speed of light in a vacuum, E_{f} is the graphene Fermi energy level, and $\hbar$ is the approximate Planck constant. From Eq. (2), one can see that the resonant frequency of the semicircle disk-patterned graphene is positively correlated with the Fermi energy level and negatively correlated with the width of graphene. In this study, the width of the graphene changes in gradient, so the plasmon resonance occurs in a wide frequency range. In addition, we control the Fermi level of graphene by DC voltage to achieve dynamic tuning of absorption characteristics. The relationship between Fermi level and DC voltage can be given by[26]

$$E_{\text{f}} = \hbar v_{\text{f}} \sqrt{\pi \varepsilon_{\text{d}} \varepsilon_0 V_{\text{g}}/e t_{\text{d}}}, \tag{3}$$

where ε_{d} is the relative dielectric constant of the dielectric layer, ε_0 is the vacuum dielectric constant, V_{g} is the applied voltage, and t_{d} is the thickness of the dielectric layer.

3. Numerical analysis

In order to study the absorption properties of the periodically semicircle-patterned graphene sheet absorber, we simulate the absorption (A), transmittance (T), reflectance (R) spectra, and the real and imaginary part of the normalized input impedance under normal incidence, when the graphene Fermi energy level is assumed to be $E_{\text{f}} = 0.6$ eV.

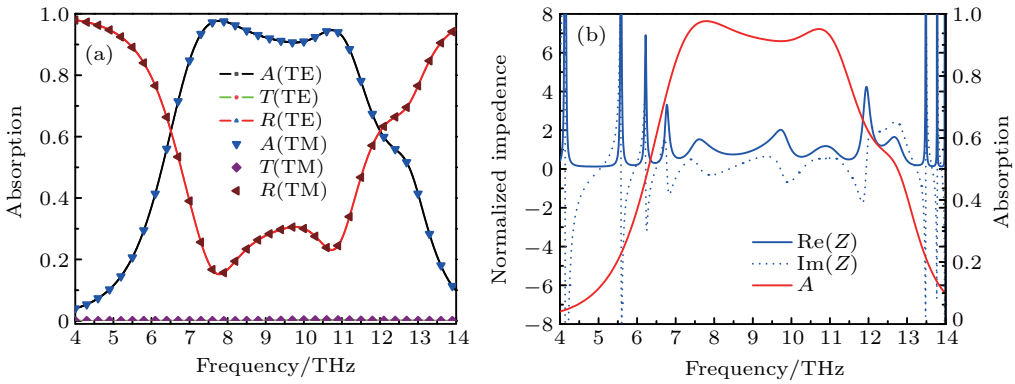


Fig. 2. (a) Absorption (A), transmittance (T), and reflectance (R) of the proposed far-infrared absorber with TE and TM modes under normal incidence, respectively, (b) the real and imaginary parts of the normalized input impedance according to the absorption spectra.

Figure 2(a) illustrates the absorption, transmittance, reflectance spectra in TE- and TM-polarized modes under far-infrared electromagnetic wave normal incidence. As expected, a broadband polarization-insensitive far-infrared absorption is achieved for both TE and TM polarizations. From the absorption, transmittance, reflectance spectra, one can see that the over 90% absorbance bandwidth reaches 4.29 THz from 6.76 THz to 11.05 THz with a central frequency of 8.905 THz for both polarizations. This indicates that the proposed absorber has the characteristics of polarization insensitive, high absorption, and broad absorbance bandwidth. Figure 2(b) displays the real and imaginary parts of the normalized input

impedance of the proposed far-infrared absorber. Because maximum absorption of the absorber occurs the impedance matching condition, which is the imaginary part of the normalized input impedance of the proposed far-infrared absorber near zero. To achieve the broad far-infrared absorbance bandwidth, the input impedance imaginary part of the proposed far-infrared absorber should be adjusted to near zero. From Fig. 2(b), we observe that the imaginary part of the proposed far-infrared absorber is near 0 from 6.76 THz to 11.05 THz. It indicates that the effective impedance of the proposed absorber matches with the free space impedance.

To investigate the absorption properties of the proposed far-infrared absorber, we analyze the absorption spectra as a function of the structural parameters h, r, and graphene Fermi levels E_f. As the dielectric layer thickness (h) of the proposed absorber increases from 4.0 μm to 5.0 μm, the absorption bandwidth exhibits slightly redshift while the dielectric layer thickness has little influence absorbance in the absorption frequency bandwidth, as shown in Fig. 3(a). As depicted in Fig. 3(b), the radius (r) of the semicircle disk patterned graphene has a significant influence on the absorbance when the parameter r varies from 1.0 μm to 1.25 μm. In order to obtain a perfect far-infrared absorber with the above 90% absorption and broad bandwidth from 6.76 THz to 11.05 THz, we set the parameter $r = 1.2$ μm. The absorption spectra of the proposed absorber under different graphene Fermi levels are plotted in Fig. 3(c). Figure 3(c) illustrates that the graphene Fermi level has a great influence on the absorption and bandwidth of the absorber. Furthermore, as the graphene Fermi levels increases from 0.2 eV to 0.7 eV, figure 3(c) clearly shows that the absorbance greatly increases from 49% to 95% and over 90% absorbance bandwidth changes from 0 THz to 4.29 THz. In the present article, we choose the geometric parameters of the proposed absorber as $h = 4.6$ μm and $r = 1.2$ μm to obtain a broad absorbance bandwidth and a high absorption.

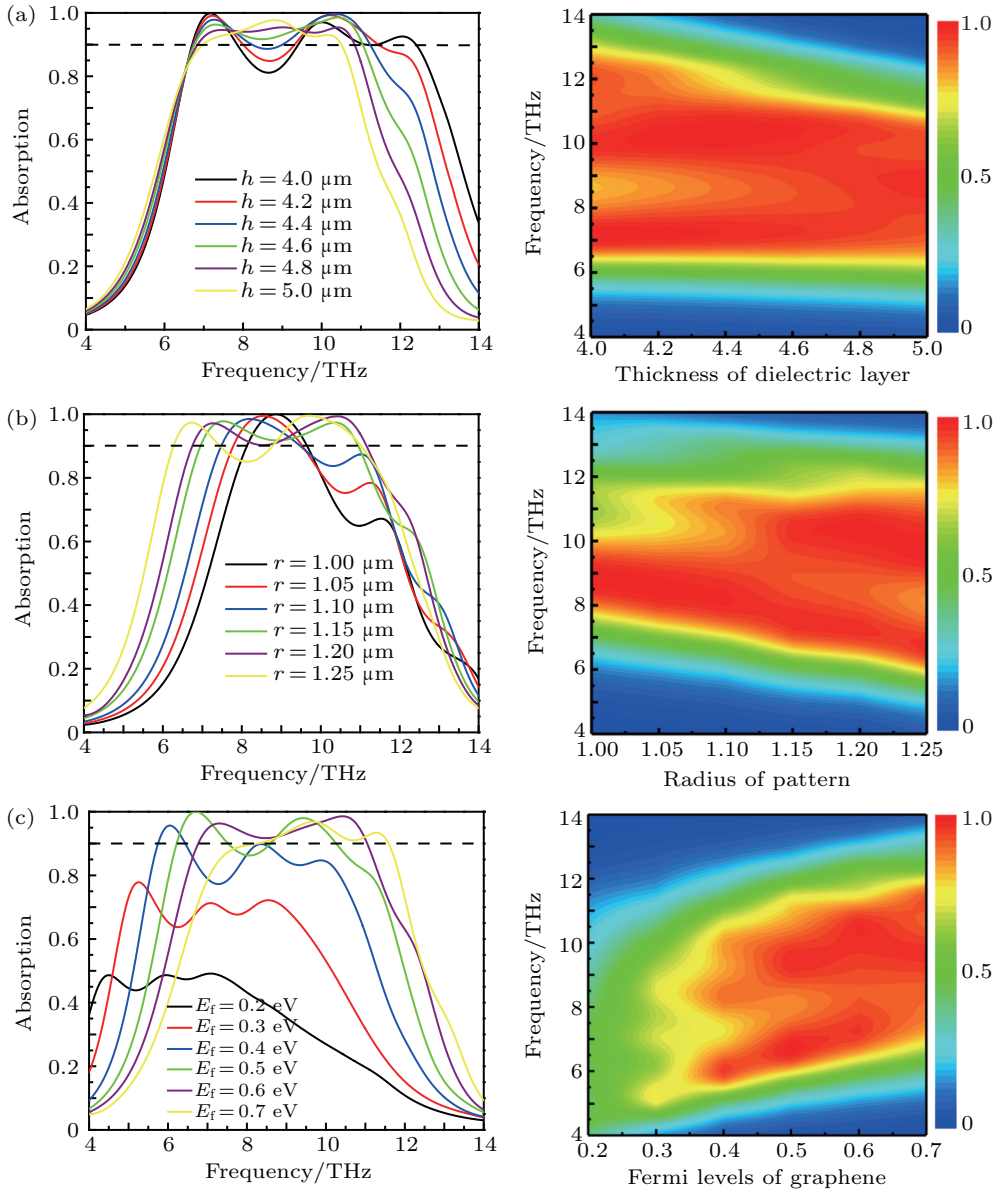


Fig. 3. Absorption spectra of the proposed far-infrared absorber with different dielectric layer thicknesses h (a), different radii r (b), and the different graphene Fermi levels E_f (c).

Figures 4(a) and 4(b) show the electric field distributions of the patterned graphene for both polarizations at the first resonant frequency of 7.78 THz. At low resonant frequency $f = 7.78$ THz, the energy is concentrated on the transverse two of semicircular patterned graphene for the TE polarization, while for the TM polarization, the energy is concentrated on the two of semicircular patterned graphene in the longitudinal direction.

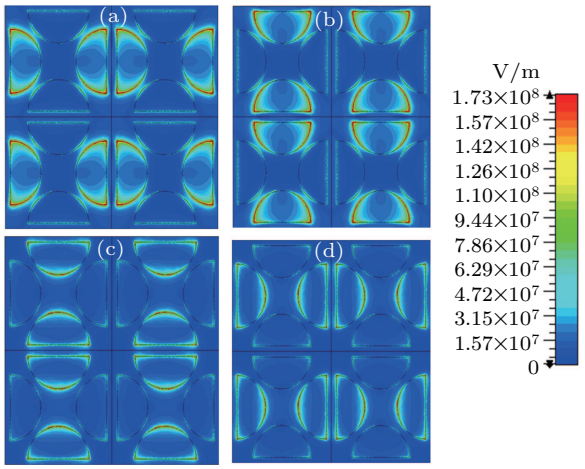


Fig. 4. Electric field distribution of (a) TE-mode and (b) TM-mode at $f = 7.78$ THz, electric field distribution of (c) TE-mode and (d) TM-mode at $f = 10.76$ THz.

Figures 4(c) and 4(d) show the electric field distributions of the patterned graphene for both polarizations at the second resonant frequency of 10.76 THz. At high resonant frequency $f = 10.76$ THz, the energy is concentrated on the longitudinal two of semicircular patterned graphene for the TE polarization, while the energy is concentrated on the transverse two of semicircular patterned graphene for the TM polarization. It is clearly observed that the energy is mainly concentrated on the edge of the graphene pattern, which means surface plasmon resonances are strongly bounded to the patterned graphene edges.

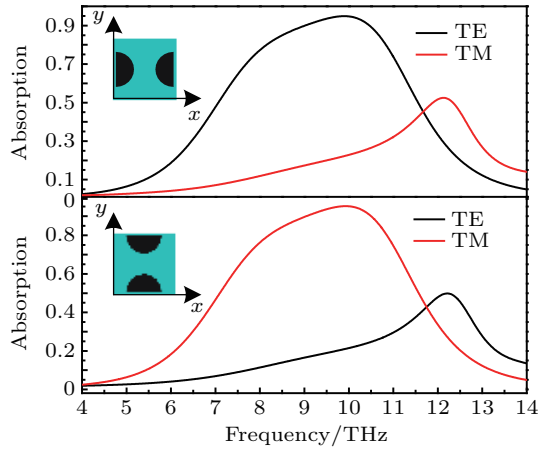


Fig. 5. Absorption spectra of different planar array directions of semicircle disk-patterned graphene and both polarizations.

Figure 5 gives the absorption spectra of different planar array directions of semicircle disk-patterned graphene and polarization modes.

Figure 6 displays the simulated power loss density and surface current distributions of the proposed absorber for TE polarization at two resonant frequencies of 7.78 THz and 10.76 THz, where figures 6(a) and 6(b) are the power loss density distributions at 7.78 THz and 10.76 THz, and figures 6(c) and 6(d) are the surface current distributions at 7.78 THz and 10.76 THz, respectively.

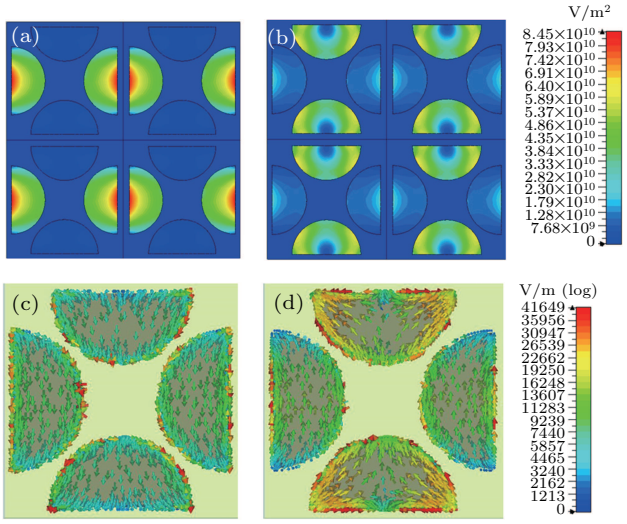


Fig. 6. Surface loss density (a) at $f = 7.78$ THz and (b) $f = 10.76$ THz, respectively; and surface current (c) at $f = 7.78$ THz and (d) $f = 10.76$ THz, respectively.

It can be noted that the proposed far-infrared absorber exhibits tight power loss density and surface current confinement around the semicircle disk-patterned graphene sheet, leading to strong far-infrared electromagnetic wave trapping and absorption. The power loss density and surface current confinement characteristics are consistent with the absorbance spectra depicted in Fig. 2. The stronger the power loss density and surface current confinement is, the higher the absorption ration of the far-infrared absorber becomes. Moreover, most of the power loss density and surface current are confined to the edge of the semicircle disk-patterned graphene due to the localized surface plasmon resonance of the patterned grapheme sheet. Specifically, the extremely confined power loss density and surface current of the TE polarization are distributed between two adjacent unit cells in y direction at low resonant frequency of 7.78 THz and x direction at high resonant frequency 10.76 THz, respectively. The physical mechanism of this phenomenon is that the electric dipole resonances between two adjacent unit cells in y and x directions are excited by the two resonant frequencies of TE polarization incident far-infrared wave, respectively. Table 1 depicts the properties of our proposed absorber and some previously reported graphene absorber. According to Table 1, one sees that the designed structure has relatively good absorption bandwidth.

Table 1. Performance comparison of our proposed absorber with some reported graphene-based absorbers.

Reference	Bandwidth > 90%/THz	Graphene type	Polarization
[11]	2.2	multilayer graphene disks and ribbons	sensitive
[27]	2.8	multiple oval graphene discs	insensitive
[28]	8.7	graphene pattern and gold pattern	insensitive
Our results	4.29	graphene semicircle disk	insensitive

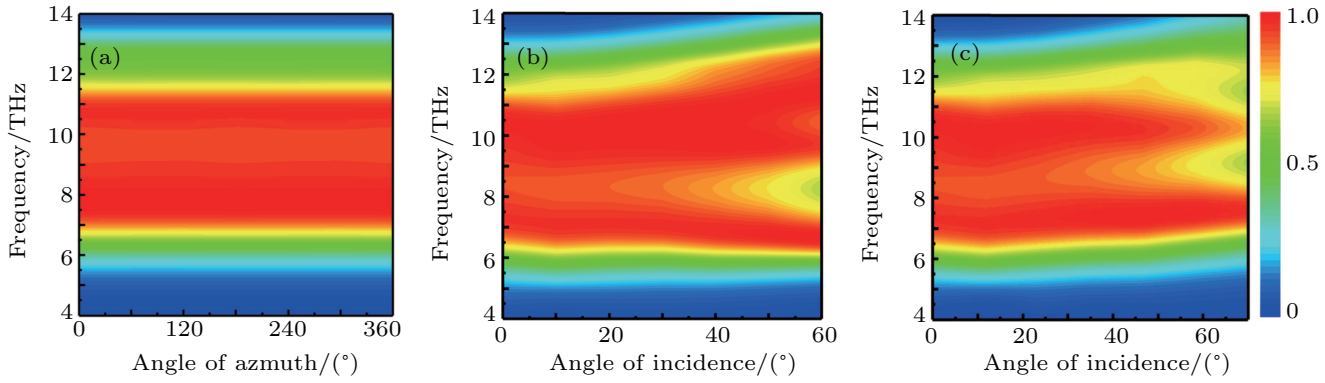


Fig. 7. Absorption spectra under (a) different azimuth angles, (b) TE-polarized mode, (c) TM-polarized mode.

Finally, the absorption behavior dependence on the polarization angle and the incident angle is further studied. Since the semicircle-patterned graphene is axisymmetrical, the polarization sensitivity of the proposed absorber can be eliminated. The dependence of the absorption spectrum on the azimuth at normal incidence is shown in Fig. 7(a). One can see that the far-infrared absorber is polarization insensitive for both TE- and TM-modes with the incident angle ranging from 0° to 360° under normal incidence electromagnetic wave. Figures 7(b) and 7(c) depict the absorption spectra as functions of operating frequency and the oblique incident angle (0°–60°) for TE- and TM-polarized modes, respectively. It can be noted that the far-infrared absorber has stable absorption bandwidth (4.29 THz) under the incident angle changing from 0° to 50° for both TE- and TM-polarizations. Since the absorption characteristics are related to the confined surface plasmon resonance, and the bandwidth of the far-infrared absorber is mainly determined by the semicircle-patterned graphene sheet, and less dependent on the incident angle. It can also be noted that the peak absorbance decreases slightly when the incident angle is near to 50° for both TE- and TM-polarizations at some frequencies in the absorption bandwidth, and the absorbance is still above 90%. Therefore, the broadband absorption of the polarization-insensitive far-infrared absorber remains more than 90% with bandwidth 4.29 THz from 6.76 THz to 11.05 THz for both TE- and TM-polarized modes at oblique incident angle of 0°–50°.

4. Conclusion

We have presented a tunable polarization-insensitive broadband far-infrared absorber based on four semicircle disk-patterned graphenes. For normal incidence, the bandwidth of 90% absorption of the polarization insensitivity absorber has reached up to 4.29 THz. When the incident angle varies from 0° to 50°, the bandwidth of 90% absorption remains more than 4.29 THz. The bandwidth and absorption can be adjusted flexibly by controlling the chemical potentials of graphene. The proposed absorber has great application prospect in sensing, detection, imaging and optoelectronic devices.

References

[1] Zhu Z, Guo C, Liu K, Zhang J, Ye W, Yuan X and Qin S 2014 *J. Appl. Phys.* **116** 104304
[2] Fang Z, Liu Z, Wang Y, Ajayan P, Nordlander P and Halas N 2012 *Nano Lett.* **12** 3808
[3] Phare C, Lee Y, Cardenas J and Lipson M 2015 *Nat. Photon.* **9** 511
[4] Li W, Chen B, Meng C, Fang W, Xiao Y, Li X, Hu Z, Xu Y, Tong L, Wang H, Liu W, Bao J and Shen Y 2014 *Nano Lett.* **14** 955
[5] Lu Z and Zhao W 2012 *Opt. Soc. Am. B* **29** 1490
[6] Liu M, Yin X, Ulin-Avila E, Geng B, Zentgraf T, Ju L, Wang F and Zhang X 2011 *Nature* **474** 64
[7] Chaharmahali I and Biabanifard S 2018 *Optik* **172** 1026
[8] Liu X, Yang H, Cui Y, Chen G, Yang Y, Wu X, Yao X, Han D, Han X, Zeng C, Guo J, Li W, Cheng G and Tong L 2016 *Sci. Rep.* **6** 26024
[9] Yao G, Ling F, Yue J, Luo C, Ji J and Yao J 2016 *Opt. Express* **24** 1518
[10] Zhang Q, Ma Q, Yan S, Wu F, He X and Jiang J 2015 *Opt. Commun.* **353** 70
[11] Biabanifard S, Biabanifard M, Asgari S, Asadi S and Yagoub M 2018 *Opt. Commun.* **427** 418
[12] Alaee R, Farhat M, Rockstuhl C and Lederer F 2012 *Opt. Express* **20** 28017

[13] Pai-Yen C and Alu A 2013 *IEEE Trans. THz Sci. Technol.* **3** 748
[14] Nikitin A, Guinea F, Garcia-Vidal F and Martin-Moreno L 2012 *Phys. Rev. B* **85** 081405
[15] Huang M, Cheng Y, Cheng Z, Chen H, Mao X and Gong R 2018 *Opt. Commun.* **415** 194
[16] Dong Y, Liu P, Yu D, Li G and Yang L 2016 *IEEE Antennas Wireless Propagat. Lett.* **16** 1115
[17] Amin M, Farhat M and BağcıH 2013 *Opt. Express* **21** 29938
[18] He S and Chen T 2013 *IEEE Trans. Terahertz Sci. Technol.* **3** 757
[19] Ke S, Wang B, Huang H, Long H, Wang K and Lu P 2015 *Opt. Express* **23** 8888
[20] Yi S, Zhou M, Shi X, Gan Q, Zi J and Yu Z 2015 *Opt. Express* **23** 10081
[21] Zhu Z, Guo C, Zhang J, Liu K, Yuan X and Qin S 2015 *Appl. Phys. Express* **8** 015102
[22] Andryieuski A and Lavrinenko A 2013 *Opt. Express* **21** 9144
[23] Ye L, Chen Y, Cai G, Liu N, Zhu J, Song Z and Liu Q 2017 *Opt. Express* **25** 11223
[24] Gao F, Zhu Z, Xu W, Zhang J, Guo C, Liu K, Yuan X and Qin S 2017 *Opt. Express* **25** 9579
[25] Grigorenko A, Polini M and Novoselov K 2012 *Nat. Photon.* **6** 749
[26] Vakil A and Engheta N 2011 *Science* **332** 1291
[27] Wu S, Zha D, Miao L, He Y and Jiang J 2019 *Phys. Scr.* **94** 105507
[28] Deng Y, Peng L, Liao X and Jiang X 2019 *Plasmonics* **14** 1057